



Study of Ag/CeO₂ catalysts for naphthalene oxidation: Balancing the oxygen availability and oxygen regeneration capacity



Minghan Liu^a, Xiaodong Wu^{a,*}, Shuang Liu^b, Yuxi Gao^a, Ze Chen^a, Yue Ma^a, Rui Ran^a, Duan Weng^a

^a Key Laboratory of Advanced Materials of Ministry of Education of China, School of Materials Science and Engineering, Tsinghua University, Beijing 100084, China

^b Institute of Materials Science and Engineering, Ocean University of China, Qingdao 266100, China

ARTICLE INFO

Article history:

Received 13 April 2017

Received in revised form 1 July 2017

Accepted 21 July 2017

Available online 22 July 2017

Keywords:

Ag/CeO₂ catalysts

Naphthalene oxidation

Cycled H₂-TPR

Oxygen availability

Oxygen regeneration capacity

ABSTRACT

A series of Ag/CeO₂ catalysts was synthesized by the incipient wetness method. Compared with Ag/Al₂O₃ and CeO₂ catalysts, Ag/CeO₂ catalysts are more promising candidates for naphthalene oxidation, in which Ce⁴⁺ act as the main active sites and are efficiently promoted by Ag species. By characterizing the solid properties and the redox ability, the mechanism of ceria catalysis by the Ag-modified catalysts was investigated. It was found that Ag species can work as an oxygen pump to enhance the oxygen availability in the ceria bulk. They also promote the oxygen regeneration capacity by the oxygen spillover effect. However, such an effect would also decrease the ability for active oxygen regeneration at higher Ag loading, which arises from the lower surface oxygen vacancy concentration. Because of the balance between these two factors, the Ag/CeO₂ catalyst with 1 wt.% Ag shows the best performance for isothermal catalytic oxidation of naphthalene.

© 2017 Elsevier B.V. All rights reserved.

1. Introduction

Polycyclic aromatic hydrocarbons (PAHs) are classified as volatile organic compounds. They are produced by combustion of organic matter such as diesel, gasoline, biomass coal, and wood [1–7]. They are harmful to both humans and the environment [8,9]. In general, there are a lot of potential control methods to remove PAHs from the atmosphere, such as adsorption, absorption, biodegradation, ozonation, thermal incineration, and catalytic oxidation [10–12]. Among these methods, catalytic oxidation is a promising technique because of its good practicability and high efficiency [13,14]. Naphthalene is the most volatile and least toxic PAH, and it also has the simplest structure [14–16]. It is considered to be a model molecule for PAHs in catalytic oxidation, and thus the information obtained from catalytic oxidation of naphthalene can be useful for abatement of other PAHs [3,17].

Commercial noble metal catalysts such as Pt/Al₂O₃ and Pd/Al₂O₃ are widely used to eliminate hazardous materials, including PAHs. However, because of their high costs, increasing attention is being paid to substitute noble metals by cheaper active phases. Metal

oxides, such as MnO_x, CoO_x, Fe₂O₃, CuO, ZnO, and CeO₂, have been shown to be effective catalysts for naphthalene oxidation. Among these metal oxides, ceria shows remarkable catalytic performance [2,17]. To further improve the catalytic activity of ceria, Ag has been introduced into ceria catalysts, resulting in Ag/CeO₂ catalysts with superior activities for oxidation of soot [18], formaldehyde [19], toluene [20] and propene [21]. Considering the much lower price of silver than other noble metals like Pt and Pd, Ag/CeO₂ catalysts are affordable in practical applications. Thus, the application potential of Ag/CeO₂ catalysts for naphthalene oxidation should be investigated in detail.

In situ characterizations and kinetic studies indicate that ceria zirconia mixed oxides catalyze oxidation of naphthalene by the Mars van Krevelen mechanism [10,22,23]. In this mechanism, there are two successive steps: the reaction between the reactant and oxygen on the surface and re-oxidation of the partly reduced surface by oxygen. In our previous studies, we showed that Ag can facilitate formation of active oxygen species by accelerating dissociation of adsorbed O₂ and migration of ceria bulk oxygen [18,24], which made contributions to the catalytic cycle. Ag also reduces the surface oxygen vacancy content of ceria. This can be explained by the electron interaction between Ag and CeO₂ (Ag⁺ + Ce³⁺ → Ag⁰ + Ce⁴⁺), which results in a low surface oxygen vacancy concentration and the formation of metallic Ag over

* Corresponding author.

E-mail address: wuxiaodong@tsinghua.edu.cn (X. Wu).

Ag/CeO₂ as detected by XPS [18,25]. On the other hand, Aranda et al. observed a direct relationship between the O_β/O_α ratio and the surface area normalized activity of Cu/CeO₂ catalysts, suggesting surface oxygen defects are important for the catalytic oxidation of naphthalene [22,26]. Thus, the reaction mechanism of naphthalene oxidation over Ag/CeO₂ and especially the roles of surface/bulk oxygen vacancy remain to be investigated.

In this study, a series of Ag/CeO₂ catalysts with different Ag loading amounts was synthesized and investigated. Activity tests and physicochemical characterizations were performed to identify the role of the Ag species and the key steps in naphthalene oxidation. The effects of the Ag content on naphthalene adsorption, the oxygen availability, oxygen regeneration, and CO₂ desorption were investigated in detail.

2. Experimental

2.1. Materials

A series of Ag/CeO₂ catalysts was prepared by the incipient wetness method using commercial CeO₂ (Brunauer–Emmett–Teller (BET) specific surface area (S_{BET}) = 180 m²/g, BASF, Germany) and AgNO₃ (99.8%, SCRC, China). CeO₂ powders were immersed in the AgNO₃ solution followed by evaporation in a rotary evaporator. The mixture was dried at 110 °C overnight and heated at 500 °C for 2 h to obtain the Ag/CeO₂ catalysts. The nominal weight ratios of Ag (counted as metallic Ag) were 0.5%, 1%, 2.5%, and 5%, and the catalysts are denoted 0.5AgCe, 1AgCe, 2.5AgCe, and 5AgCe, respectively. As reference samples, CeO₂ and Ag/Al₂O₃ catalysts were also prepared by a similar process replacing the AgNO₃ solution and CeO₂ with distilled water and Al₂O₃ (S_{BET} = 150 m²/g, BASF), respectively. The Ag loading in the Ag/Al₂O₃ catalyst was 1 wt.%, and the catalyst is denoted 1AgAl.

2.2. Catalytic activities

The naphthalene conversion experiments were performed in a micro-reactor. The sample (100 mg, 30–60 mesh) sandwiched by the quartz pool was placed in the middle of the quartz tube. The inlet stream was 120 ppm naphthalene with 10% O₂ balanced by N₂ to simply simulate the combustion emissions [16]. The total gas flow rate was 400 ml/min (gas hourly space velocity (GHSV) = 175,000 h⁻¹). Gas chromatography with flame ionization detector (GC-FID, 7890B, Agilent, US) was applied to measure the concentration of naphthalene in the outlet gas. The tests were performed in the temperature range 160–300 °C (with a temperature interval 20 °C). It took about 1 h for the concentration of naphthalene in the outlet gas reached the equilibrium value. After then five consistent analyses were used to minimize the system errors. A blank test was performed without any catalysts in the quartz tube, and the result showed that spontaneous oxidation of naphthalene would not occur at temperatures below 300 °C. Naphthalene conversion is defined as

$$\text{Naphthalene conversion}_T = \frac{[\text{NAP}]_0 - [\text{NAP}]_T}{[\text{NAP}]_0} \quad (1)$$

where [NAP]₀ is the inlet concentration of naphthalene and [NAP]_T is the outlet concentration of naphthalene at reaction temperature T.

In order to evaluate the activity of the catalysts for total oxidation of naphthalene, an infrared spectrometer (Thermo Nicolet, iS10, USA) was employed to measure the CO₂ produced in the isothermal experiment. The yield to CO₂ is defined as

$$[\text{Yield to CO}_2]_T = \frac{[\text{CO}_2]_T}{10[\text{NAP}]_0} \quad (2)$$

where the [NAP]₀ is the inlet concentration of naphthalene and [CO₂]_T is the outlet concentration of CO₂ at reaction temperature T.

2.3. Characterizations

X-ray powder diffraction (XRD) of the products was performed using a Bragg–Brentano-type powder diffractometer (D8 ADVANCE, Bruker, Germany, operated at 40 kV and 30 mA, Cu K α radiation, λ = 0.15418 nm). The X-ray diffractograms were recorded at 0.01 intervals in the range 20° to 80° with a scanning velocity of 6°/min. In addition, step scanning XRD analysis was performed with the same instrument in the range 37.5° to 39.5° with a scanning velocity of 0.2°/min. The crystallite size of ceria was calculated by Scherrer equation.

The sample morphologies were observed by transmission electron microscopy (JEOL 2100 with an accelerating voltage of 200 kV and a point resolution of 0.19 nm) and N₂ adsorption–desorption isotherms were determined at –196 °C (JW-BK122F, Beijing JWGB, China). The BET and BJH method was used to calculate the specific surface areas and the pore volumes of the samples, respectively.

The actual Ag contents in the catalysts were measured by an inductively coupled plasma optical emission spectroscopy (IRIS Intrepid II XSP, Thermo, USA).

X-ray photoelectron spectroscopy (XPS) was performed with a multifunctional imaging electron spectrometer (ESCALAB 250XI, Thermo, USA) equipped with a monochromatic Al K α (1486.6 eV) X-ray source. The binding energy of C 1 s (284.8 eV) was used as the internal standard. The spectra were fitted using the XPSPEAK program by curve fitting with Gaussian functions after subtraction of the Shirley-type background.

Raman spectroscopy (IDSpec J300, Aurora, China) was performed at room temperature and normal atmosphere pressure. An argon ion laser with a wavelength of 532 nm was used to scan the sample surface. The wavenumber values in the Raman spectra are accurate to 4 cm⁻¹.

Naphthalene temperature-programmed desorption (NAP-TPD) was performed by GC-FID (7890B, Agilent, US). Before the tests, the samples (100 mg) were heated in N₂ flow (400 ml/min) at 300 °C for 30 min to perform proper degassing. After cooling to 100 °C, the catalysts were exposed to 120 ppm naphthalene vapor balanced with N₂ (400 ml/min) for 30 min and flushed with N₂ (400 ml/min) for 30 min. The NAP-TPD profiles were then obtained by heating the samples from 100 to 350 °C at 5 °C/min in N₂ flow (400 ml/min).

CO₂ temperature-programmed desorption (CO₂-TPD) was performed on a Micromeritics AutoChem II 2920. Prior to the measurements, the samples were degassed at 400 °C for 30 min in He. During the CO₂ adsorption process, the catalysts were exposed to CO₂ (50 ml/min) at 25 °C for 30 min and flushed with He (50 ml/min) until the baseline of the TCD signal was stable. The CO₂ desorption curves were obtained by heating the samples from 25 to 300 °C at 10 °C/min in He flow (50 ml/min).

Cycled H₂ temperature-programmed reduction (cycled H₂-TPR) was performed to further investigate the redox ability of the catalysts. The experimental procedure is shown in Fig. 1. According to our previous work, all of the active oxygen species in the Ag/CeO₂ catalysts can be removed by H₂ below 300 °C [18]. After pre-redox treatment, four rounds of H₂-TPR were performed to reveal the redox behavior of the catalysts in detail. We paid close attention to the results of the first and fourth rounds because

- According to our previous study, Ag can facilitate migration of bulk oxygen atoms in ceria [18], forming active oxygen species (O[•]). The reactivity between O[•] and H₂ can be used to evaluate the reactivity between O[•] and naphthalene, so the reduction tem-

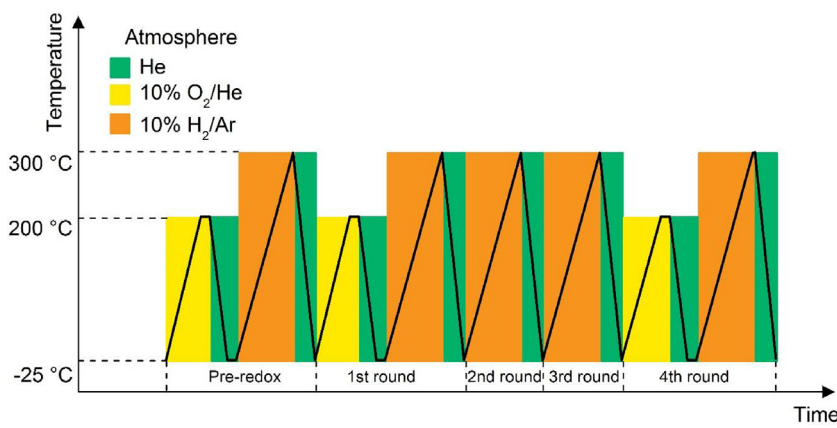


Fig. 1. Experimental procedure for cycled H₂-TPR.

perature in the first round of H₂-TPR can be used to estimate the availability of oxygen species in the different catalysts.

- After being heated several times in 10% H₂/Ar, migration of ceria bulk oxygen atoms in Ag/CeO₂ catalysts is drastically inhibited [24], which means that H₂ consumption in the fourth round of H₂-TPR can be completely attributed to O[•], which is formed during the pre-oxidizing process. Consequently, H₂ consumption in the fourth round of H₂-TPR can be used to estimate regeneration of oxygen species from gaseous O₂.

3. Results

3.1. Naphthalene oxidation activity

The conversion curves for isothermal catalytic oxidation of naphthalene are shown in Fig. 2a. The activity of the catalysts is in the order Ag/CeO₂ > CeO₂ » Ag/Al₂O₃. It appears that ceria is an active catalyst for naphthalene oxidation, with complete conversion achieved at 300 °C. The Ag-modified catalysts exhibit significantly improved activities with gaseous naphthalene being completely eliminated at 240 °C. Their superior activities do not originate mainly from the silver species because the 1AgAl catalyst is almost inert with the maximum naphthalene conversion lower than 5% at 300 °C. The effect of the Ag loading amount on naphthalene oxidation is clear. The activity of the Ag/CeO₂ catalysts follows the order 1AgCe > 2.5AgCe ≈ 0.5AgCe > 5AgCe. The optimal loading of Ag is 1 wt.%, and the light-off temperature (T_{50}) of this catalyst is around 175 °C.

Almost no CO is observed in the outlet gas when using the IR gas analyzer as the monitoring instrument. The yield to CO₂ curves of Ag/CeO₂ and CeO₂ catalysts are shown in Fig. 2b. The CO₂ selectivity (CO₂/CO_x) in the whole temperature range is always higher than 99%. The comparison of naphthalene conversion and CO₂ production indicates a deficit in carbon balance. It is ascribed to the formation of by-products since the catalytic activity results were obtained after the equilibrium of the naphthalene adsorption [27]. According to the CO₂ production results, the activity sequence of the Ag/CeO₂ catalysts turns to be 1AgCe ≈ 2.5AgCe > 0.5AgCe > 5AgCe.

The gap between naphthalene conversion and yield to CO₂ shows that although Ag/CeO₂ catalysts are highly active for naphthalene oxidation, complete oxidation to CO₂ is not achieved when the temperature is lower than 240 °C. Generally, the carbon deficit (yield to CO₂ is lower than naphthalene conversion) can be attributed to naphthalene adsorption and/or by-product formation [27]. In the isothermal experiment, the deficit only depends on the formation of by-products once the adsorption-desorption equilibrium is reached at a certain temperature. Besides, the resource of

CO₂ is rather complex. It can be produced not only by the partial and complete oxidation of naphthalene but also by that of intermediate products [27,28]. Here, naphthalene conversion was chosen to evaluate the activity of the catalysts in the following discussion. Besides, selectivity for naphthalene to CO₂ profiles were printed in Fig. S1.

Moreover, considering there is always a certain amount of water vapor in the real reaction condition, the influence of water on the catalyst activity should be considered. Since the chromatography column employed in this study was not waterproof, an infrared spectrometer was employed to obtain CO₂ concentrations in the outlet gas when introducing 5% H₂O in naphthalene catalytic oxidation test. As shown in Fig. S2, water can slightly facilitate the

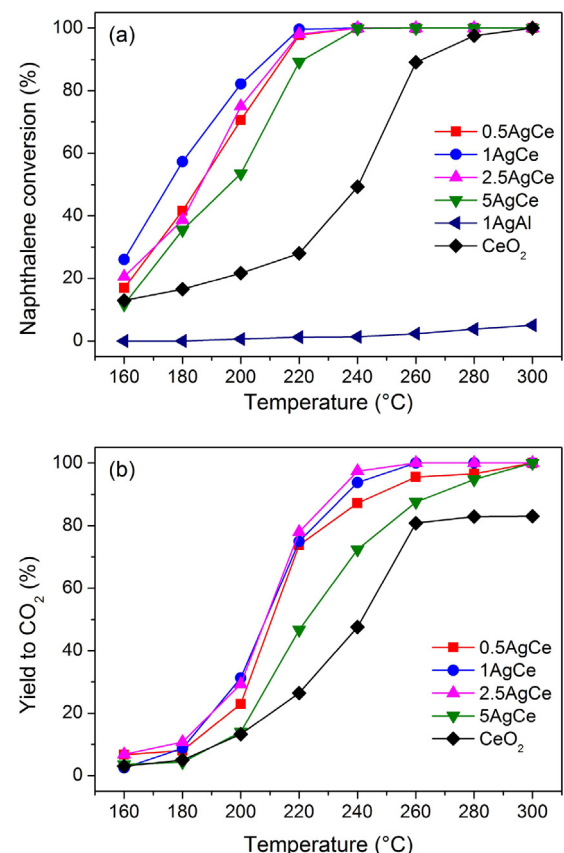


Fig. 2. (a) Naphthalene conversion and (b) Yield to CO₂ in catalytic oxidation of naphthalene. Reaction conditions: 120 ppm naphthalene, 10% O₂ and N₂ in balance, GHSV = 175,000 h⁻¹.

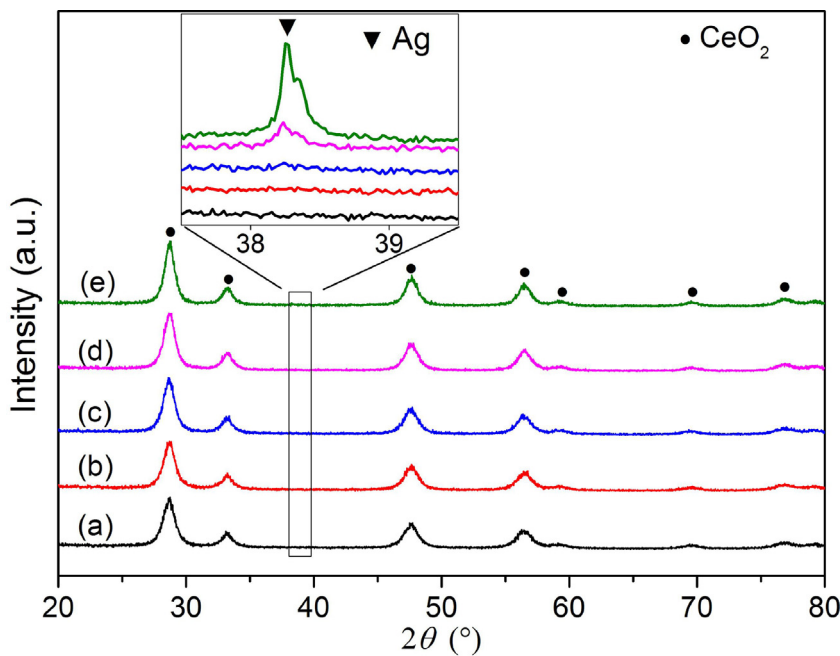


Fig. 3. XRD patterns of (a) CeO_2 , (b) 0.5AgCe, (c) 1AgCe, (d) 2.5AgCe, and (e) 5AgCe.

Table 1

Summary of the solid properties of the CeO_2 and Ag/ CeO_2 catalysts.

Catalyst	D_{CeO_2} (nm) ^a	S_{BET} ($\text{m}^2 \cdot \text{g}^{-1}$) ^b	V_{pore} ($\text{cm}^3 \cdot \text{g}^{-1}$) ^b	CO_2 adsorption ($\text{mmol} \cdot \text{g}^{-1}$) ^c	
				Physisorbed	Chemisorbed
CeO_2	8.6	178	0.0757	0.63	0.07
0.5AgCe	8.7	154	0.0642	0.53	0.06
1AgCe	8.7	143	0.0537	0.46	0.04
2.5AgCe	9.1	117	0.0438	0.37	0.02
5AgCe	10.2	111	0.0417	0.32	0.04

^a Crystallite size of ceria calculated from the XRD data by the Scherrer equation.

^b Specific surface areas and pore volumes calculated by BET and BJH method, respectively.

^c Obtained from CO_2 -TPD.

catalytic oxidation of naphthalene over 1AgCe. Due to the weak influence of water vapor, the following results and discussion were made based on naphthalene oxidation reactions in the dry atmosphere.

3.2. Solid properties

Fig. 3 shows the XRD patterns of the CeO_2 and Ag/ CeO_2 catalysts. The intense peaks of fluorite CeO_2 are present in all of the patterns [21,25,29,30]. The ceria crystallite size was calculated, and the results are given in Table 1. No shift of the diffraction peaks of ceria occurs with Ag loading, indicating that silver does not enter into the ceria lattice. No characteristic peaks of Ag or Ag_2O are present. However, the step scanning XRD profiles in the inset figure indicate crystallization of metallic silver on the different catalysts. The diffraction peak assigned to metallic Ag at $2\theta = 38.2^\circ$ (JCPDS No. 65-2871) gradually increases with increasing Ag loading.

The specific surface areas and pore volumes of the CeO_2 and Ag/ CeO_2 catalysts obtained from the N_2 adsorption–desorption isotherms are listed in Table 1. Commercial CeO_2 has a high specific surface area of $178 \text{ m}^2/\text{g}$. The BET surface areas of the Ag modified catalysts decrease with increasing metal loading owing to the accelerated calcination effect of Ag on ceria [18,19,25]. Besides, as shown in Fig. S3, introducing Ag can cause the loss of mesopores in the catalysts, especially the pores with the diameter lower than

5 nm. The collapse of the support pore structure is related to the introduction of the metal as well.

High-resolution transmission electron microscopy (HRTEM) was performed to investigate the morphologies of the catalysts (Fig. 4). It is difficult to observe any Ag particles in the images of 0.5AgCe and 1AgCe because of the high dispersion of the precious metal. Only the (111) and (100) planes of CeO_2 can be clearly identified. Metallic Ag particles are observed for the high-loaded catalysts (i.e., 2.5AgCe and 5AgCe). These results correlate well with the step scanning XRD results.

ICP-OES analysis was recorded to evaluate the Ag content in the series of Ag/ CeO_2 catalysts. As listed in Table 2, the actual Ag loading in the catalysts only has minor difference with the nominal Ag loading. Because the catalysts were prepared via an incipient wetness method, 100% of the added Ag was expected to be presented on the supports [31].

3.3. XPS and Raman spectra

XPS spectra were recorded to obtain chemical information about the elements on the surface, including the chemical valences of Ag and Ce and surface oxygen vacancy surface ($\text{O}_{\text{v-s}}$) content. The Ce 3d spectra of the CeO_2 and Ag/ CeO_2 catalysts are shown in Fig. 5a. After deconvolution, six peaks related to Ce^{4+} 3d (ν_{1-6} : 882.5, 888.5, 898.3, 901.0, 907.5, and 916.8 eV) and four peaks related to Ce^{3+} 3d (ν_{1-4} : 881.5, 884.5, 899.8, and 902.8 eV) were obtained [18,21,29].

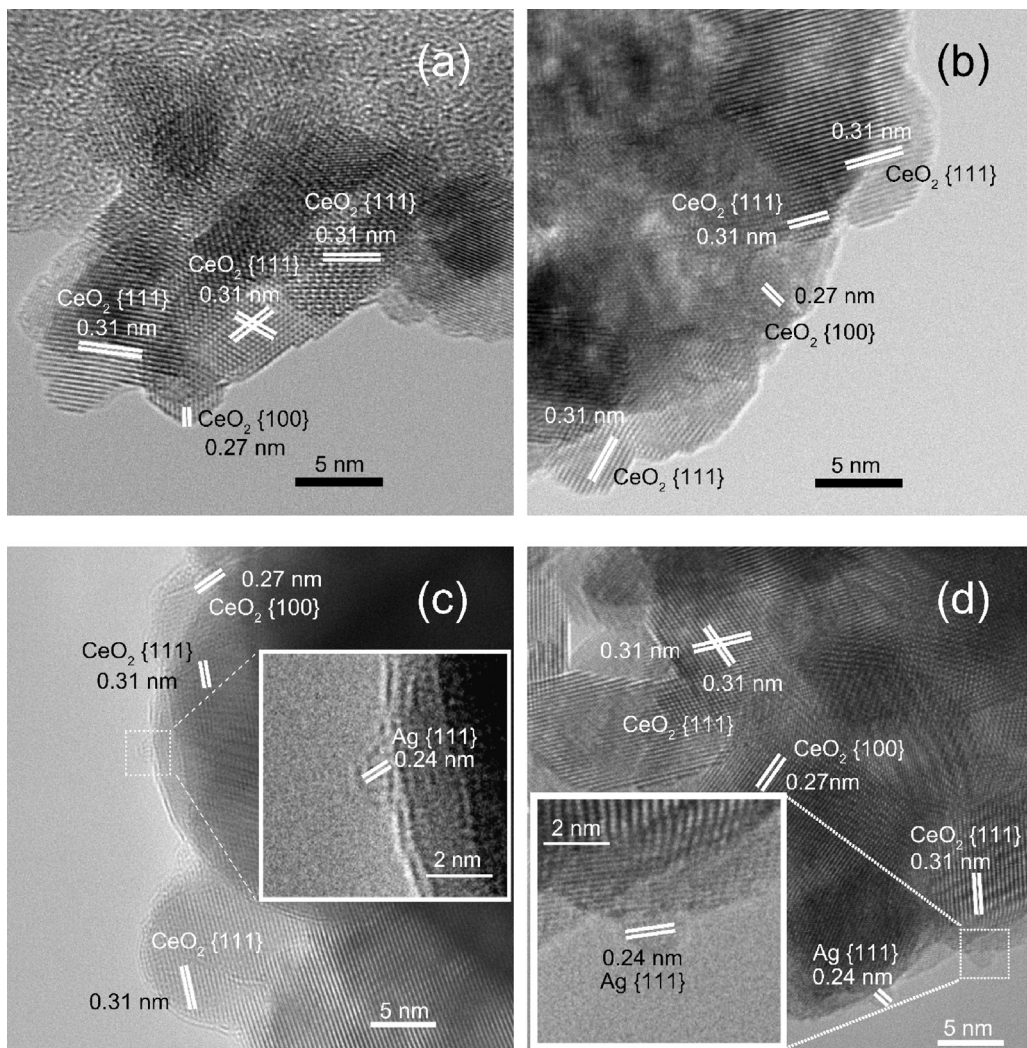


Fig. 4. HRTEM images of (a) 0.5AgCe, (b) 1AgCe, (c) 2.5AgCe, and (d) 5AgCe.

Table 2Chemical states of the CeO₂ and Ag/CeO₂ catalysts.

Catalyst	Actual (Nominal) Ag content (%) ^a	Ce ³⁺ /Ce ⁴⁺ ratio on surface ^b	Ag ⁰ /(Ag ⁰ + Ag ^{δ+}) on surface ^b	Wavenumber of F _{2g} band ^c (cm ⁻¹)	I _d /I _{F2g} ^c
CeO ₂	/	0.56	/	469	0.047
0.5AgCe	0.5(0.5)	0.47	0.72	464	0.077
1AgCe	1.0(1.0)	0.44	0.73	464	0.085
2.5AgCe	2.4(2.5)	0.43	0.81	459	0.100
5AgCe	5.1(5.0)	0.30	0.99	455	0.104

^a Obtained by ICP-OES analysis.^b Obtained from the XPS data.^c Obtained from the Raman spectra.

Ag loading appears to decrease the surface Ce³⁺/Ce⁴⁺ ratio (Table 2). The corresponding mechanism has been discussed in our previous study and Luches et al.'s study [18,32]. Because formation of oxygen vacancies is highly related to the presence of Ce³⁺ [33], the O_{v-s} content follows the same order as the O 1s spectra in Fig. S4.

The Ag 3d spectra of the Ag/CeO₂ catalysts are shown in Fig. 5b, in which two peaks assigned to Ag^{δ+} (367.5 and 373.5 eV) and two peaks assigned to Ag⁰ (368.1 and 374.1 eV) are obtained after deconvolution [25,34,35]. The ratio of metallic Ag on the catalyst surface was calculated by [Ag⁰]/([Ag⁰] + [Ag^{δ+}]). Metallic Ag is dominant on all of the Ag/CeO₂ catalysts (Table 2), and the Ag species tend to exist in the metallic form with high Ag loading, which is

possibly because of the increase in the size of the Ag nanoparticles [36].

Raman spectroscopy was used to reveal the influence of loading silver on the lattice oxygen defects. Fig. 6 shows the Raman spectra of the CeO₂ and Ag/CeO₂ catalysts. The Raman bands at around 470 and 598 cm⁻¹ correspond to vibration of the F_{2g} symmetry and defect-induced modes (D), respectively [4,25,37,38]. The F_{2g} band exhibits an obvious red shift after Ag loading (see Table 2), suggesting reduction of ceria in the bulk. Furthermore, considering the intensity of the F_{2g} band as an internal standard, quantitative interpretation of the bulk oxygen vacancy (O_{v-b}) content can be performed by calculating I_d/I_{F2g}, where I_d and I_{F2g} are the intensi-

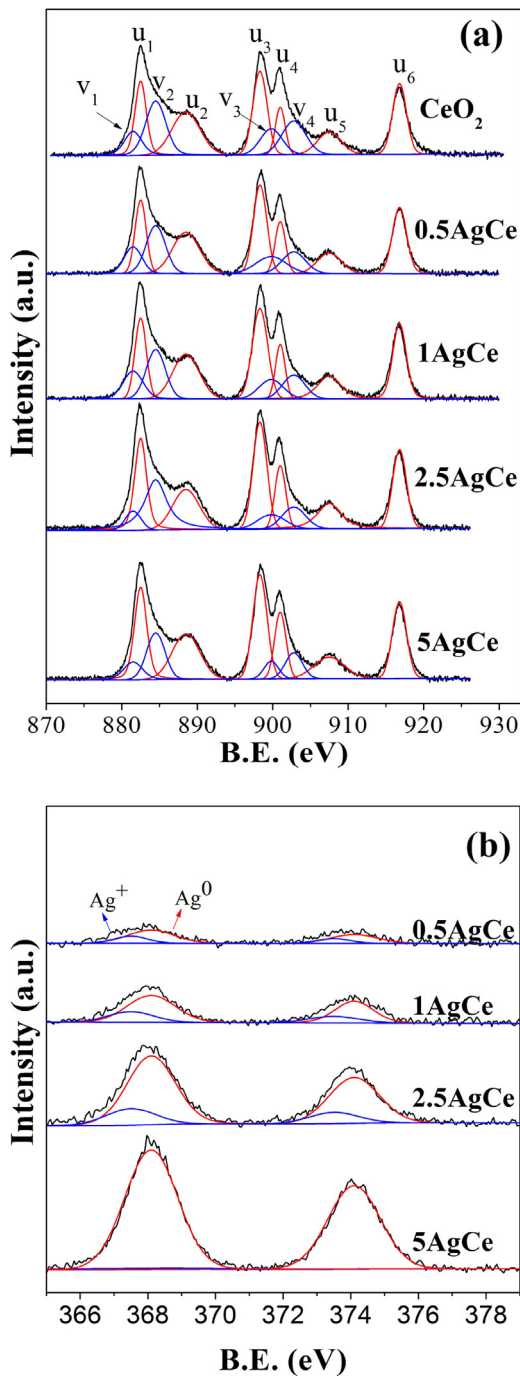


Fig. 5. (a) Ce 3d and (b) Ag 3d XPS spectra of the Ag/CeO₂ catalysts.

ties of the D and F_{2g} bands, respectively [38]. As shown in Table 2, the O_{v-b} content is in the order 5AgCe > 2.5AgCe > 1AgCe > 0.5AgCe > CeO₂, which is in agreement with production of Ce³⁺ in the bulk.

XPS and Raman results can characterize surface and bulk oxygen vacancies, respectively. Considering the inverse trends of these two oxygen vacancies with the silver loading, the oxygen reverse spillover effect by Ag can be deduced. The decrease of the Ce³⁺ concentration on the surface is attributed to compensation of surface oxygen vacancies by the migration of deeper oxygen atoms, which is promoted by oxygen reverse spillover of Ag [39,40]. Meanwhile, extra bulk oxygen vacancies are generated because of migration of bulk oxygen atoms towards the surface.

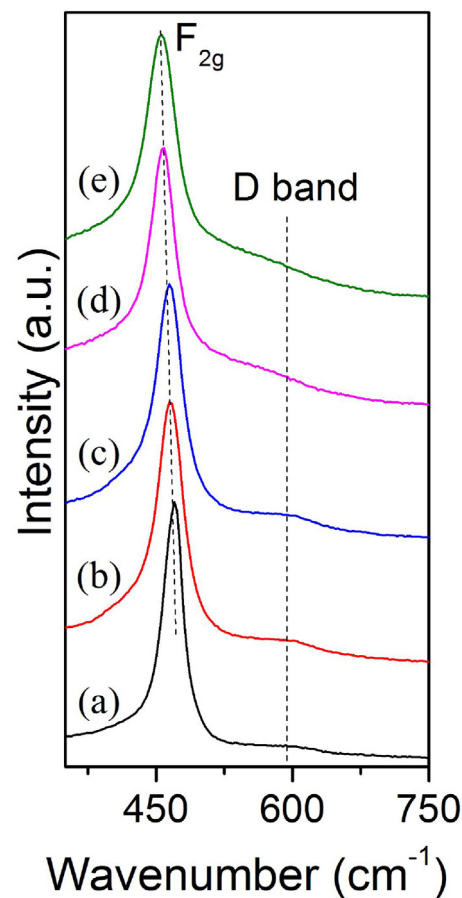


Fig. 6. Raman spectra of (a) CeO₂, (b) 0.5AgCe, (c) 1AgCe, (d) 2.5AgCe, and (e) 5AgCe.

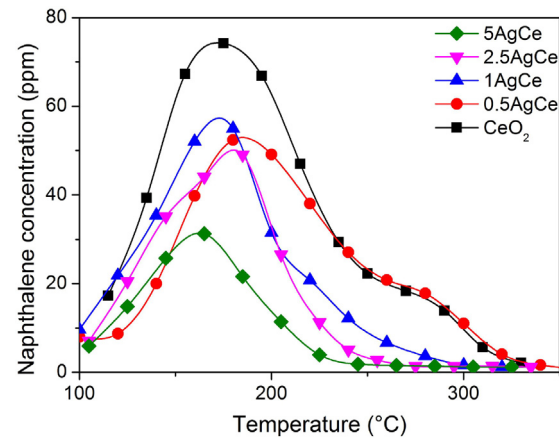


Fig. 7. Naphthalene TPD profiles of the catalysts.

3.4. NAP-TPD

Catalytic oxidation of naphthalene is a typical heterogeneous reaction, in which adsorption of the reactant can be an important step. Therefore, NAP-TPD profiles were obtained to investigate the influence of the Ag amount on the naphthalene adsorption capacity (Fig. 7). There are two main desorption peaks at 180 (LT) and 270 °C (HT) in the profile of CeO₂, representing weakly and strongly adsorbed naphthalene on the surface of the catalyst, respectively. In the profile of 0.5AgCe, the LT peak becomes weaker while the HT peak is unchanged. With increasing Ag loading, both the desorption peaks decrease in intensity and shift towards lower temperatures.

Table 3
Overview of naphthalene desorption in NAP-TPD.

Catalyst	Amount of desorbed naphthalene	
	Total (mmol·g ⁻¹)	Normalized (μmol·m ⁻²)
CeO ₂	0.28	1.55
0.5AgCe	0.21	1.37
1AgCe	0.18	1.23
2.5AgCe	0.14	1.22
5AgCe	0.08	0.76

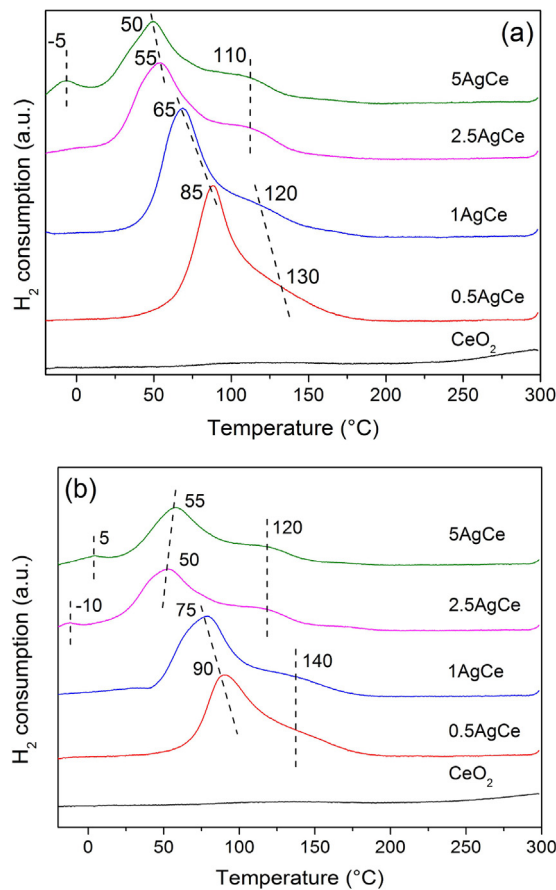


Fig. 8. Profiles of the (a) first and (b) fourth rounds of cycled H₂-TPR.

The HT peak is not present in the profile of 5AgCe. The amount of the desorbed naphthalene was calculated and normalized with the specific surface area of the catalyst. As listed in Table 3, the total amount of naphthalene desorption over the catalyst decreased with the loading of silver. It can be seen from the order of the normalized amount per m² of ceria that the NAP adsorption depends strongly on the specific surface area of the catalyst except 5AgCe. Other factors such as pore structure of ceria also have influences on the adsorption of naphthalene [2].

3.5. H₂-TPR

The redox behavior of catalysts is crucial in Mars van Krevelen reactions. TPR tests were performed with different experimental conditions to investigate the effect of loading Ag on the reducibility of CeO₂. As mentioned in Section 2.3, the first and fourth rounds of H₂-TPR are used to characterize the oxygen availability and oxygen regeneration ability of the catalysts. According to the results of the first round of H₂-TPR shown in Fig. 8a, reduction of surface oxygen in CeO₂ occurs above 300 °C while consumption of H₂ occurs mainly below 200 °C for all of the Ag/CeO₂ catalysts, revealing that

the migration of ceria bulk oxygen to the surface is significantly accelerated by the participant of silver through a reverse spillover effect [39,40]. In the H₂-TPR profile of 0.5AgCe, there are two main intense H₂ consumption peaks at 85 and 130 °C, which mainly represent active oxygen species (O[•]) near Ag and O[•] far away from Ag, respectively [18]. With increasing Ag loading, both of the peaks shift towards lower temperature, indicating that increasing the Ag loading results in better availability of O[•] atoms. In particular, the total O[•] (calculated according to the H₂ consumption) content is much larger than that from reduction of Ag₂O to Ag even if all of the Ag was in the form of Ag₂O. Therefore, the increased O[•] content in the Ag/CeO₂ catalysts should not only be attributed to silver oxides. In fact, according to our previous studies [18,24] and the experimental results in this work (see Fig. S5a), formation of O[•] is because of migration of ceria bulk oxygen atoms to the surface.

Migration of ceria bulk oxygen atoms in Ag/CeO₂ catalysts would be drastically inhibited after being heated several times in 10% H₂/Ar, which is confirmed by the result of the third round H₂-TPR (see Fig. S5b). Thus, almost all the O[•] measured in the fourth round of H₂-TPR can be attributed to the regenerated oxygen from the gaseous O₂ during the pre-oxidizing treatment, and the O[•] regeneration capacity can be estimated by the hydrogen consumption in the fourth round of H₂-TPR. Almost no reduction peak is observed in the profile of CeO₂ at the temperatures lower than 300 °C. Compared with ceria, O[•] can be effectively regenerated for the Ag/CeO₂ catalysts in an oxidizing atmosphere at 200 °C. As shown in Fig. 8b, the fourth round H₂-TPR profiles of the Ag/CeO₂ catalysts contain two intense reduction peaks, which are also related to O[•] with different distances from the Ag species [18]. Additionally, a weak peak at around 0 °C is present in the profiles of 2.5AgCe and 5AgCe. This peak may be assigned to reduction of superoxide species near to Ag [18]. The contributions of cationic silver and ceria to the total H₂ consumption were estimated, respectively. The amount of cationic silver on the catalysts was calculated based on the results of ICP and XPS, and hence the theoretical H₂ consumption for the reduction of Ag₂O can be given in Table 4. It can be seen that the O[•] species on ceria are dominant compared with those on Ag₂O. The O[•] content in the catalysts follows the order 0.5AgCe > 1AgCe > 2.5AgCe > 5AgCe (>> CeO₂). It appears that extra Ag reduces the ability of O[•] regeneration in the CeO₂ lattice.

In summary, introduction of Ag can greatly improve the redox property of the catalysts, and extra Ag loading results in better oxygen availability but poorer active oxygen regeneration capacity.

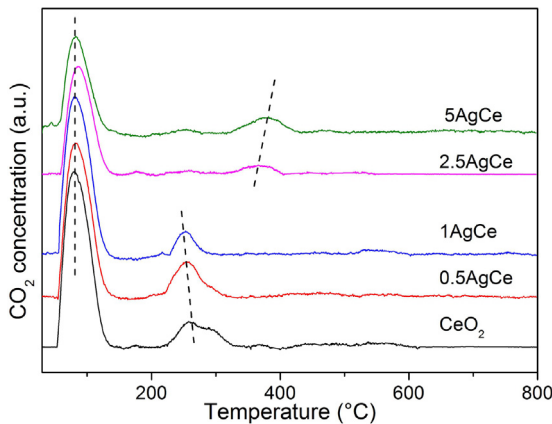
3.6. CO₂-TPD

Desorption of the products is generally believed to be one of the most important steps in the Mars van Krevelen reaction. CO₂ (the main product of naphthalene oxidation) can adsorb on ceria, which is a typical base oxide [4]. Physically adsorbed CO₂, chemisorbed CO₂, and formation of carbonate species have a negative effect on the catalytic activity. CO₂-TPD patterns were obtained to investigate the effect of Ag loading on the CO₂ adsorption ability (Fig. 9). There is a sharp CO₂ desorption peak at 80 °C in the profiles of all of the catalysts. As shown in Table 1, CO₂ desorption is in the order CeO₂ > 0.5AgCe > 1AgCe > 2.5AgCe > 5AgCe, which is the same order as the BET surface area. Based on the desorption temperatures and agreement with the surface areas, these peaks are suggested to represent CO₂ physically adsorbed on the surface.

In Fig. 9, there are small CO₂ desorption peaks at temperatures higher than 200 °C, which are attributed to chemisorbed CO₂. CO₂ chemisorbed on CeO₂ desorbs in a wide temperature range with a peak at 265 °C. With introduction of 0.5% and 1% Ag, the peak shifts to lower temperatures of 260 and 255 °C, respectively. Furthermore, the peak area decreases for both 0.5AgCe and 1AgCe. When the Ag content increases to 2.5% and 5%, the peak at around 260 °C

Table 4H₂ consumption in the fourth round H₂-TPR.

Catalyst	Total H ₂ consumptions (mmol·g ⁻¹) ^a	H ₂ consumed by Ag ₂ O (mmol·g ⁻¹) ^b	H ₂ consumed by ceria (mmol·g ⁻¹) ^c
0.5AgCe	0.56	0.006	0.55
1AgCe	0.52	0.012	0.51
2.5AgCe	0.48	0.022	0.46
5AgCe	0.46	0.002	0.46

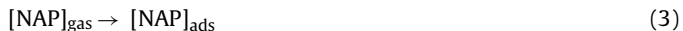
^a Obtained from the fourth round H₂-TPR.^b Theoretical values based on the results of Ag 3d XPS and ICP-OES.^c Obtained by subtracting the contribution of Ag₂O reduction.**Fig. 9.** CO₂-TPD profiles of the catalysts.

becomes quite weak, suggesting that chemisorption of CO₂ on CeO₂ is inhibited. In addition, there is an additional CO₂ desorption peak at 370 and 380 °C in the profiles of 2.5AgCe and 5AgCe, respectively. These peaks are believed to be related to CO₂ chemisorbed on Ag particles [41].

Thus, Ag modification can inhibit physical adsorption of CO₂, prevent CO₂ from chemisorbing on CeO₂, and facilitate desorption of CO₂. Moreover, on the high Ag-loaded catalysts, there are more Ag particles, which act as new CO₂ chemisorption sites and CO₂ chemisorbs with higher thermal stability.

4. Discussion

Even though Ag/Al₂O₃ can both bind naphthalene and dissociate O₂ to form active oxygen species [42,43], it is almost inert for naphthalene oxidation according to the activity tests in this work. Therefore, catalytic oxidation of naphthalene with the Ag/CeO₂ catalysts probably follows the Mars van Krevelen mechanism. Because of the lack of redox ability, Ag/Al₂O₃ can hardly complete the catalytic cycle. The reaction is suggested to follow the steps



Eq. (3) represents adsorption of gaseous naphthalene on the catalyst. Eq. (4) is the reaction of adsorbed naphthalene and the active oxygen species. Eq. (5) is desorption of the main product (CO₂). Eq. (6) represents regeneration of active oxygen as well as re-oxidation of the reduced catalyst. Similar reaction mechanisms have been suggested for naphthalene oxidation on CeO₂-ZrO₂ catalysts and CO/toluene oxidation on Au/CeO₂ catalysts [10,44–46]. In the following sections, we discuss the catalytic cycle and the role of the Ag species in the Ag/CeO₂ catalysts.

4.1. Adsorption of naphthalene and desorption of CO₂

In the Mars van Krevelen reaction, adsorption of reactant molecules (Eq. (3)) is a crucial step, so the naphthalene adsorption ability is important in catalytic oxidation of naphthalene [10]. This viewpoint is supported by studies of catalytic oxidation of other aromatic hydrocarbons [47–49]. As shown by the NAP-TPD results, introduction of Ag decreases the capability of ceria to adsorb gaseous naphthalene. Moreover, the BET surface area decreases with increasing Ag loading, which is in agreement with the naphthalene adsorption ability. It appears that adsorption of naphthalene on the Ag/CeO₂ catalysts mainly depends on the Ce sites. However, as shown in Fig. S6, 1AgAl shows similar naphthalene adsorption ability to 1AgCe and CeO₂, but it can hardly catalyze oxidation of naphthalene. Therefore, although loading of Ag inhibits adsorption of naphthalene on ceria to some extent, the negative effect is not decisive in naphthalene oxidation.

Generally, the products can occupy the active sites of catalysts, causing deactivation of the catalysts [4]. Therefore, desorption of CO₂ should be considered in catalytic oxidation of naphthalene. As shown by CO₂-TPD, loading Ag can decrease physically adsorbed CO₂ on the catalyst. However, it is unlikely to influence naphthalene oxidation because the desorption temperature of the physically adsorbed CO₂ is much lower than the reaction temperature. Thus, we considered chemisorbed CO₂ in this work. As suggested by previous studies [50,51], chemisorbed CO₂ join with oxygen vacancies on the ceria surface, and pre-oxidation on ceria can suppress chemisorption of CO₂. With increasing Ag loading, the oxygen vacancy content on the ceria surface decreases, so chemisorption of CO₂ on ceria also decreases. However, increasing the Ag loading also promotes formation of Ag nanoparticles, which can act as chemisorption sites for CO₂ [41]. On one hand, the CO₂ chemisorbed on ceria can form carbonate groups, which are inert for catalytic oxidation of naphthalene [4]. On the other hand, owing to adsorptive competition with O₂, the CO₂ chemisorbed to Ag is unfavorable for oxygen regeneration. Therefore, proper Ag loading would be favorable for minimizing the total amount of chemisorbed CO₂. However, deactivation of the catalysts was not observed during an isothermal experiment at 200 °C for 1.5 h (see Fig. S7). Thus, the influence of CO₂ adsorption can be ignored.

4.2. Oxygen availability and oxygen regeneration capacity

Studies of Ag-supported catalysts have suggested that Ag species can efficiently dissociate adsorbed O₂ to produce active oxygen species [52,53], so both 1AgCe and 1AgAl have the ability to dissociate oxygen molecules. The low reducibility is believed to be the most possible reason why 1AgAl is inactive in naphthalene oxidation (see Fig. S8). This indicates that the redox cycle of the catalyst is probably the rate-determining step in naphthalene oxidation by the Mars van Krevelen mechanism.

The reaction between the adsorbed reactant and active oxygen in the catalyst (Eq. (4)) is one of the most significant steps in the Mars van Krevelen mechanism. According to the results in this work as well as previous studies [18,24], the bulk oxygen in ceria can be

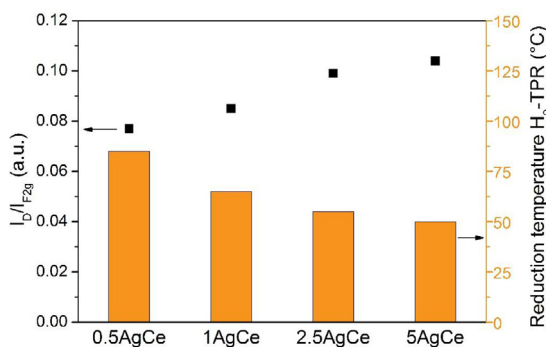


Fig. 10. Correlation between the O_{v-b} content and the active oxygen availability. The oxygen availability is represented by the reduction temperature of O[•] in the first round of H₂-TPR.

more efficiently used with the assistance of Ag. On one hand, the oxygen atoms in the ceria lattice can migrate to the surface, transforming to O[•] [24,40]. Migration of oxygen can be facilitated by the reverse spillover effect of metallic Ag, which works as an oxygen pump [18,40]. On the other hand, the O_{v-b} concentration increases because of preferential oxygen transfer towards the surface, promoting the oxygen mobility. The oxygen mobility in the bulk can be improved because of the increase in the O_{v-b} content [39,54], further promoting the utility of the lattice oxygen in ceria. According to Xu et al.'s study of Ag/MnO₂ catalysts, highly dispersed Ag exhibits a high oxygen reverse spillover ability [55]. Luches et al.'s study also suggested that the oxygen reverse spillover effect is not pronounced with large Ag nanoparticles [32]. As indicated by XRD, Ag dispersion in the different Ag/CeO₂ catalysts is in the order 0.5AgCe ≈ 1AgCe > 2.5AgCe > 5AgCe, which is not in agreement with the reduction temperature in H₂-TPR. Therefore, the oxygen availability in the Ag/CeO₂ catalysts is more likely to depend on other factors. According to the agreement between the O_{v-b} content and the reduction temperature in the first round of H₂-TPR, it is more likely that the oxygen availability in the Ag/CeO₂ catalysts is controlled by the oxygen mobility in bulk ceria (see Fig. 10). The oxygen reverse spillover ability is apparently less important than the O_{v-b} content, possibly because transfer of bulk oxygen is a slow step and may be the rate-determining step.

The re-oxidation step of reduced ceria, in which regeneration of active oxygen occurs, has been suggested to be one of the most important steps in catalytic oxidation of naphthalene [10]. The oxygen regeneration capacities of the catalysts were evaluated by the fourth round of cycled H₂-TPR. The oxygen regeneration capacity follows the order 0.5AgCe > 1AgCe > 2.5AgCe > 5AgCe ≈ CeO₂. The fact that Ag can assist dissociation of oxygen molecules has been shown by experimental phenomena and theoretical calculations [42,43,56]. Oxygen spillover by noble metals is influenced by various factors, such as the dispersion effect, chemical bonding, and the charging effect [57,58], although it is not clear in this work. By oxygen isotope analysis of Pt/CeO₂ catalysts for CO oxidation, Holmgren et al. showed that adsorption of oxygen rather than the oxygen spillover step is the rate-determining step during regeneration of oxygen in the catalysts [59]. As indicated by the XPS results, the O_{v-s} content decreases with increasing Ag loading. These oxygen vacancies may act as a passage for oxygen transfer. Therefore, because 5AgCe has the lowest O_{v-s} content, it has the lowest oxygen regeneration ability among the catalysts. As shown in Fig. 11, the O_{v-s} content plays a decisive role in the oxygen regeneration capacity of the Ag/CeO₂ catalysts.

Consequently, introduction of Ag can significantly improve the redox ability, including the oxygen availability and oxygen regeneration capacity. Owing to the reverse spillover effect, the overloaded Ag species leads to an increase in bulk oxygen vacancies and a

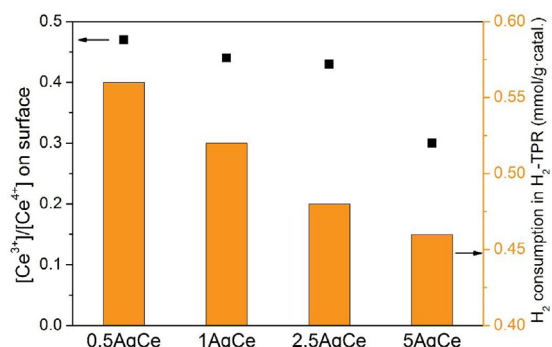


Fig. 11. Correlation between the O_{v-s} concentration and the active oxygen regeneration capacity. The active oxygen regeneration capacity is represented by the total H₂ consumption in the fourth round of H₂-TPR.

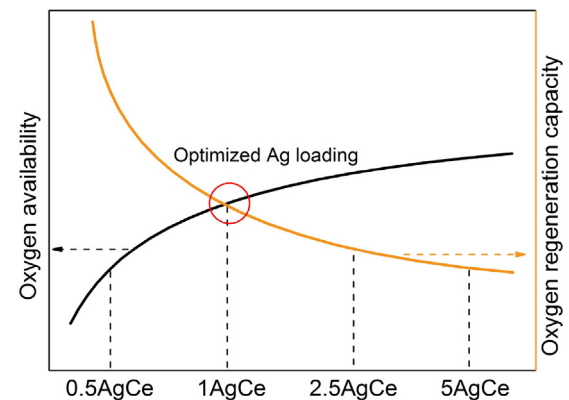


Fig. 12. Balance between the oxygen availability and the oxygen regeneration capacity in the series of Ag/CeO₂ catalysts.

decrease in surface oxygen vacancies, which are the dominant factors for the oxygen availability and oxygen regeneration capacity, respectively. The correlation between the Ag loading and the naphthalene oxidation activity is determined by the opposite influences of these two main factors. Proper Ag loading (1 wt.%) is the balance between the oxygen availability and the oxygen regeneration capacity, and the catalyst with proper Ag loading shows the best catalytic performance for naphthalene oxidation under the specific experimental conditions in this work (Fig. 12).

5. Conclusions

In this work, CeO₂ and Ag/CeO₂ catalysts with different Ag contents were investigated for catalytic oxidation of naphthalene. The mechanism of Ag modification is as follows:

- Catalytic oxidation of naphthalene over the Ag/CeO₂ catalysts complies with the Mars van Krevelen mechanism, in which the oxygen availability and oxygen regeneration capacity are the most important factors. Adsorption of naphthalene and desorption of CO₂ do not appear to be important steps in the reaction.
- Introduction of Ag to CeO₂ increases the oxygen availability and oxygen regeneration capacity. The former factor is strongly related to the number of oxygen vacancies in bulk ceria and can be strongly promoted with metallic Ag by the reverse spillover effect. The latter factor mainly depends on the number of oxygen vacancies on the ceria surface, which is restricted by introduction of Ag.
- Under the specific conditions in this work, the Ag/CeO₂ catalyst with 1 wt.% Ag shows the best catalytic activity for naphthalene

oxidation because of the optimal balance between the above two factors. The light-off temperature is 175 °C.

Acknowledgements

This work was supported by the Ministry of Science and Technology of China (project numbers 2016YFC02052 and 2015AA034603) and the China Post-doctoral Science Foundation (project number 2015M580607). We would also like to acknowledge financial support from the National Key R&D Program of China and Key Laboratory of Advanced Materials of the Ministry of Education of China and Key Academic Institutions Open Fund from School of Environment Tsinghua University.

Appendix A. Supplementary data

Supplementary data associated with this article can be found, in the online version, at <http://dx.doi.org/10.1016/j.apcatb.2017.07.058>.

References

- [1] J. Shie, C. Chang, J. Chen, W. Tsai, Y. Chen, C. Chiou, C. Chang, *Appl. Catal. B* 58 (2005) 289–297.
- [2] T. García, B. Solsona, S.H. Taylor, *Appl. Catal. B* 66 (2006) 92–99.
- [3] E. Ntatinjua N, S.H. Taylor, *Top. Catal.* 52 (2009) 528–541.
- [4] D.R. Sellick, A. Aranda, T. García, J.M. López, B. Solsona, A.M. Mastral, D.J. Morgan, A.F. Carley, S.H. Taylor, *Appl. Catal. B* 132–133 (2013) 98–106.
- [5] G. Yıldız, F. Ronse, R. Venderbosch, R.V. Duren, S.R.A. Kersten, W. Prins, *Appl. Catal. B* 168–169 (2015) 203–211.
- [6] S. Chitsazan, S. Sepehri, G. Garbarino, M.M. Carnasciali, G. Busca, *Appl. Catal. B* 187 (2016) 386–398.
- [7] G. Corro, E. Vidal, S. Cebada, U. Pal, F. Bañuelos, D. Vargas, E. Guilleminot, *Appl. Catal. B* 216 (2017) 1–10.
- [8] S.C. Marie-Rose, T. Belin, J. Mijoin, E. Fiani, M. Taralunga, F. Nicol, X. Chaucherie, P. Magnoux, *Appl. Catal. B* 90 (2009) 489–496.
- [9] J. Bünger, J. Krahl, A. Weigel, O. Schröder, T. Brüning, M. Müller, E. Hallier, G. Westphal, *Arch. Toxicol.* 80 (2006) 540–546.
- [10] A. Bampenrat, V. Meeyoo, B. Kitiyanan, P. Rangsuvigit, T. Rirkosomboon, *Catal. Commun.* 9 (2008) 2349–2352.
- [11] E.N. Ndifor, T. García, S.H. Taylor, *Catal. Lett.* 110 (2006) 125–128.
- [12] A.M. Mastral, T. García, M.S. Callén, J.M. López, M.V. Navarro, R. Murillo, J. Galbán, *Environ. Sci. Technol.* 36 (2002) 1821–1826.
- [13] Y. Li, X. Zhang, H. He, Y. Yu, T. Yuan, Z. Tian, J. Wang, Y. Li, *Appl. Catal. B* 89 (2009) 659–664.
- [14] J. Park, J. Lee, J. Miyawaki, W. Pang, S. Yoon, I. Mochida, *Catal. Commun.* 11 (2010) 1068–1071.
- [15] E.N. Ndifor, T. García, B. Solsona, S.H. Taylor, *Appl. Catal. B* 76 (2007) 248–256.
- [16] M. Ferrandon, E. Björnbom, *J. Catal.* 200 (2001) 148–159.
- [17] B. Puertolas, B. Solsona, S. Agouram, R. Murillo, A.M. Mastral, A. Aranda, S.H. Taylor, T. García, *Appl. Catal. B* 93 (2010) 395–405.
- [18] S. Liu, X. Wu, W. Liu, W. Chen, R. Ran, M. Li, D. Weng, *J. Catal.* 337 (2016) 188–198.
- [19] L. Ma, D. Wang, J. Li, B. Bai, L. Fu, Y. Li, *Appl. Catal. B* 148–149 (2014) 36–43.
- [20] S. Scirè, P.M. Riccobene, C. Crisafulli, *Appl. Catal. B* 101 (2010) 109–117.
- [21] M. Skaf, S. Aouad, S. Hany, R. Cousin, E. Abi-Aad, A. Aboukaïs, *J. Catal.* 320 (2014) 137–146.
- [22] A. Aranda, S. Agouram, J.M. López, A.M. Mastral, D.R. Sellick, B. Solsona, S.H. Taylor, T. García, *Appl. Catal. B* 127 (2012) 77–88.
- [23] P. Mars, D.W. van Krevelen, *Chem. Eng. Sci.* 3 (1954) 41–59.
- [24] Y. Gao, A. Duan, S. Liu, X. Wu, W. Liu, M. Li, S. Chen, X. Wang, D. Weng, *Appl. Catal. B* 203 (2017) 116–126.
- [25] S. Chang, M. Li, Q. Hua, L. Zhang, Y. Ma, B. Ye, W. Huang, *J. Catal.* 293 (2012) 195–204.
- [26] A. Aranda, E. Aylon, B. Solsona, R. Murillo, A.M. Mastral, D.R. Sellick, S. Agouram, T. García, S.H. Taylor, *Chem. Commun.* 48 (2012) 4704–4706.
- [27] T. García, B. Solsona, D. Cazorlaamoros, A. Linaressolano, S. Taylor, *Appl. Catal. B* 62 (2006) 66–76.
- [28] F. Diehl, J. Barbier Jr, D. Duprez, I. Guibard, G. Mabilon, *Appl. Catal. B* 95 (2010) 217–227.
- [29] Z. Qu, F. Yu, X. Zhang, Y. Wang, J. Gao, *J. Chem Eng* 229 (2013) 522–532.
- [30] H. Huang, Q. Dai, X. Wang, *Appl. Catal. B* 158–159 (2014) 96–105.
- [31] B. Azambre, S. Collura, P. Darcy, J.M. Trichard, P. Da Costa, A. García-García, A. Bueno-López, *Fuel Process. Technol.* 92 (2011) 363–371.
- [32] P. Luches, F. Pagliuca, S. Valeri, F. Illas, G. Preda, G. Pacchioni, *J. Phys. Chem. C* 116 (2012) 1122–1132.
- [33] A. Trovarelli, *Catal. Rev.* 38 (1996) 439–520.
- [34] C. Lee, J.-I. Park, Y.-G. Shul, H. Einaga, Y. Teraoka, *Appl. Catal. B* 174–175 (2015) 185–192.
- [35] H. Deng, Y. Yu, F. Liu, J. Ma, Y. Zhang, H. He, *ACS Catal.* 4 (2014) 2776–2784.
- [36] F. Benedetti, P. Luches, M.C. Spadaro, G. Gasperi, S. D'Addato, S. Valeri, F. Boscherini, *J. Phys. Chem. C* 119 (2015) 6024–6032.
- [37] P. Yang, S. Yang, Z. Shi, Z. Meng, R. Zhou, *Appl. Catal. B* 162 (2015) 227–235.
- [38] H. Huang, Y. Gu, J. Zhao, X. Wang, *J. Catal.* 326 (2015) 54–68.
- [39] S. Hu, W. Wang, Y. Wang, Q. Xu, J. Zhu, *J. Phys. Chem. C* 119 (2015) 18257–18266.
- [40] S. Hu, Y. Wang, W. Wang, Y. Han, Q. Fan, X. Feng, Q. Xu, J. Zhu, *J. Phys. Chem. C* 119 (2015) 3579–3588.
- [41] X. Guo, R.J. Madix, *J. Phys. Chem. B* 105 (2001) 3878–3885.
- [42] J.R. Hahn, W. Ho, *J. Chem. Phys.* 123 (2005) 214702.
- [43] W.H. Thijssen, D. Marjenburgh, R.H. Bremmer, J.M. van Ruitenbeek, *Phys. Rev. Lett.* 96 (2006) 026806.
- [44] S. Scirè, S. Minicò, C. Crisafulli, C. Satriano, A. Pistone, *Appl. Catal. B* 40 (2003) 43–49.
- [45] V. Shapovalov, H. Metiu, *J. Catal.* 245 (2007) 205–214.
- [46] H.Y. Kim, G. Henkelman, *J. Phys. Chem. Lett.* 4 (2013) 216–221.
- [47] A.A. Barresi, G. Baldi, *Ind. Eng. Chem. Res.* 33 (1994) 2964–2974.
- [48] C. Wang, S. Lin, *Appl. Catal. A* 268 (2004) 227–233.
- [49] Y.T. Lai, T.C. Chen, Y.K. Lan, B.S. Chen, J.H. You, C.M. Yang, N.C. Lai, J.H. Wu, C.S. Chen, *ACS Catal.* 4 (2014) 3824–3836.
- [50] T. Jin, Y. Zhou, G.J. Mains, J.M. White, *J. Phys. Chem.* 91 (1987) 5931–5937.
- [51] Z. Cheng, B.J. Sherman, C.S. Lo, *J. Chem. Phys.* 138 (2013) 014702.
- [52] A. Palermo, A. Husain, M.S. Tikhov, R.M. Lambert, *J. Catal.* 207 (2002) 331–340.
- [53] K. Villani, R. Brosius, J. Martens, *J. Catal.* 236 (2005) 172–175.
- [54] N.V. Skorodumova, S.I. Simak, B.I. Lundqvist, I.A. Abrikosov, B. Johansson, *Phys. Rev. Lett.* 89 (2002) 166601.
- [55] R. Xu, X. Wang, D. Wang, K. Zhou, Y. Li, *J. Catal.* 237 (2006) 426–430.
- [56] J. Wang, M. Liu, M. Lin, *Solid State Ionics* 177 (2006) 939–947.
- [57] D. Guo, Q. Guo, K. Zheng, E.G. Wang, X. Bao, *J. Phys. Chem. C* 111 (2007) 3981–3985.
- [58] C. Descorme, D. Duprez, *Appl. Catal. A* 202 (2000) 231–241.
- [59] A. Holmgren, D. Duprez, B. Andersson, *J. Catal.* 182 (1999) 441–448.